4746 *Macromolecules* **2009**, *42*, 4746–4750
DOI: 10.1021/ma900199t

Macromolecules
ARTICLE

Branch Content of Metallocene Polyethylene

Ramnath Ramachandran, Gregory Beaucage,* and Amit S. Kulkarni

Department of Chemical and Materials Engineering, University of Cincinnati, Cincinnati, Ohio 45221

Douglas McFaddin, Jean Merrick-Mack, and Vassilios Galiatsatos

Equistar Chemicals, LP, a LyondellBasell Company, Cincinnati Technology Center, 11530 Northlake Drive, Cincinnati, Ohio 45249

Received January 29, 2009; Revised Manuscript Received May 14, 2009

ABSTRACT: Small-angle neutron scattering (SANS) is employed to investigate the structure and long-chain branch (LCB) content of metallocene-catalyzed polyethylene (PE). A novel scaling approach is applied to SANS data to determine the mole fraction branch content (ϕ_{br}) of LCBs in PE. The approach also provides the average number of branch sites per chain (n_{br}) and the average number of branch sites per minimum path ($n_{br,p}$). These results yield the average branch length (z_{br}) and number of inner segments n_i, giving further insight into the chain architecture. The approach elucidates the relationship between the structure and rheological properties of branched polymers. This SANS method is the sole analytic measure of branch-on-branch structure and average branch length for topologically complex macromolecules.

Introduction

Structural branching is known to occur in a variety of materials such as polymers and ceramic aggregates.[1,2] Owing to the influence of branching on the physical and chemical properties of these materials, a universal technique to quantify the branch content has long been sought. Branching in polymers can be classified into short-chain branching (SCB), referring to branches that have only a few carbon atoms and are much smaller than the backbone to which they are attached, and long-chain branching (LCB) where the length of the branch is comparable to that of the backbone. The effects of short-chain branching have been discussed previously.[3] A new scaling model[4] has recently been developed to quantify long-chain branch content in such ramified structures. The scaling model has been employed successfully to study ceramic aggregates[4] and to describe the folded and unfolded state in proteins and RNA.[5] This model can be used to quantify long-chain branching in polymers as well. Long-chain branching has significant influence on the physical properties displayed by a polymer. The presence of long-chain branches (LCBs) considerably affects the structure and consequently the rheological properties and processability of polymers.[6−9] Hence, an efficient and comprehensive method to quantify long-chain branch (LCB) content in polymers has been desired for many years. Various techniques based on size-exclusion chromatography (SEC),[10] nuclear magnetic resonance (NMR) spectroscopy,[11] and rheology[12,13] have been utilized to determine LCB content in branched polymers. The drawbacks of these existing techniques have been previously discussed.[14] SEC is ineffective in characterizing low levels of LCB. NMR cannot distinguish between short- and long-chain branches, and rheological estimates of LCB, though sensitive to low levels of LCB, tend to be semiempirical and qualitative in nature.[14] However, NMR is an effective technique to determine the total number of branch sites (β) in some polymer chains. In this paper, a scaling model[4] is applied to small-angle neutron scattering (SANS) data obtained from dilute solutions of metallocene polyethylene samples to quantify the LCB content in polymers. These samples have been previously studied in the literature.[12,13] New data provided from this model will allow polymer chemists to better understand rheological consequences of polymer structures while developing new catalysts for complex polymer architectures.

A polyethylene (PE) chain can be considered to exhibit two structural levels: the overall radius of gyration R_g with mass fractal dimension d_f and the substructural rodlike persistence length l_p or Kuhn length $l_k = 2l_p$.[15] These features can be observed in a small-angle scattering pattern and can be determined through the application of local scattering laws and mass-fractal power laws under the Rayleigh−Gans approximation. Local scattering laws such as Guinier's law and power laws describe these levels. Guinier's law is given by[16]

$$I(q) = G \exp\left(\frac{-q^2 R_g{}^2}{3}\right) \tag{1}$$

where I(q) is the scattered intensity, scattering vector $q = 4\pi \sin(\theta/2)/\lambda$, θ is the scattering angle, λ is the wavelength of radiation, R_g is the coil radius of gyration, and G is defined as $N_p n_p{}^2$, where N_p is the number density of polymer coils, and n_p the square of the difference in neutron scattering length density between coil and solvent times the square of the volume of the coil. The mass-fractal power law is another local scattering law.

$$I(q) = B_f q^{-d_f} \quad \text{for } 1 \le d_f < 3 \tag{2}$$

It describes a mass-fractal object of dimension d_f, where B_f is the power law prefactor. Together, they give an account of local features like size (R_g and l_p) and surface/mass scaling.[4,17,18] The unified function developed by Beaucage,[3,17−19] used here, is useful to examine small-angle scattering data from fractal structures with multiple structural levels such as carbon nanotubes[20] and polyethylene.

*Corresponding author.

 Published on Web 06/05/2009

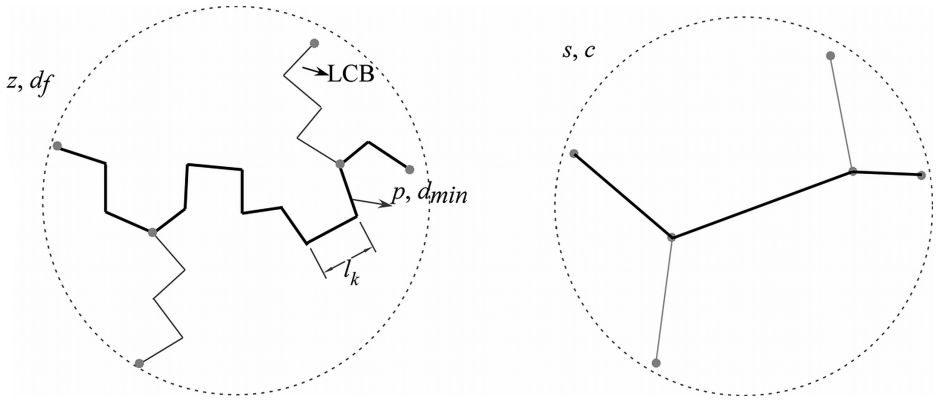

Figure 1. (a, left) Schematic of a branched polymer. The polymer is composed of Kuhn steps of length l_k. The dark lines represent an average minimum path p of dimension d_{min}. The lighter lines represent the long-chain branches. (b, right) Connective path represented by straight lines connecting branch points and free ends (gray dots), of total size s and connectivity dimension c.

Beaucage[4] has described a scaling model which can be employed to quantify branch content in polymers. A branched polymer chain of size $R_{g,2}$ is considered to be composed of z freely jointed Kuhn steps each of size l_k[3,19] as shown in Figure 1a.

The structure of the branched polymer can further be decomposed into an average minimum path p (number of Kuhn steps in the minimum path) through the structure as shown in Figure 1a. p is an average traversing path through the chain structure. A scaling relationship can be proposed between z and p[4]

$$z = p^c = s^{d_{min}} \tag{3}$$

where c is the connectivity dimension assuming the scaling prefactor to be one. The minimum path p is a mass-fractal of dimension d_{min} and size $r \sim p^{1/d_{min}}$ while the total chain of z Kuhn steps has a dimension $d_f \geq d_{min}$ and the same size $r \sim z^{1/d_f}$. A parameter s (eq 3) can also be defined using d_{min} that reflects the number of steps required to connect all branch points and end points in the polymer structure by straight lines (size $r \sim s^{1/c}$). Substituting $p \sim r^{d_{min}}$ in eq 3 and comparing with $z \sim r^{d_f}$ yields $d_f = cd_{min}$, which shows that the chain scaling (d_f, z) can be decomposed into contributions from chain tortuosity (d_{min}, p) and chain connectivity (c, s). For a linear polymer chain $d_{min} = d_f$ and $c = 1$. On the other hand, for a completely branched object like a sphere or a disk, where a linear minimum path can be traversed, $d_f = c$ and $d_{min} = 1$. The minimum path dimension, d_{min}, and connectivity dimension c represent different features of the branched chain. While c increases with increased branching or connectivity, d_{min} increases with tortuosity in the chain, driven by the thermodynamics in a dilute polymer solution. That is, for a linear chain in good solvent $d_{min} = 5/3$ and $c = 1$. For a branched chain, $1 < c \leq d_f$ and $1 \leq d_{min} \leq 5/3$. d_{min} deviates from 5/3 because the minimum path can find shortcuts through the branched structure. From the scaling model, the mole fraction branches (ϕ_{br}) is given by[4]

$$\phi_{br} = \frac{z - p}{z} = 1 - z^{(1/c)-1} \tag{4}$$

Equations 1 and 2 can be used to calculate d_f, c, p, and s. d_{min} can be calculated from[3,4]

$$d_{min} = \frac{B_f R_{g,2}^{d_f}}{C_p \Gamma\left(\frac{d_f}{2}\right) G} \tag{5}$$

where C_p is the polydispersity factor[3,21] and Γ is the gamma function. The quantities in eqs 4 and 5 can be acquired from small-angle neutron scattering (SANS) data from dilute hydrogenous polymer solutions in deuterated solvent fit to the unified function which is given by[3,17,18]

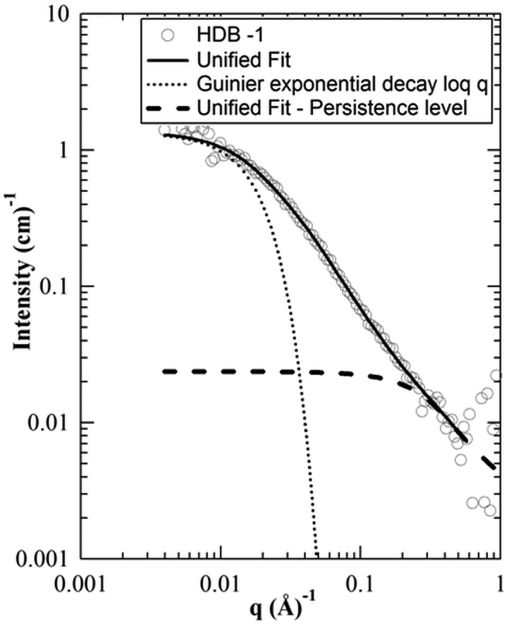

Figure 2. SANS data for sample HDB-1 fit to the unified fit.[17,18] Data shown above were obtained at IPNS.

$$I(q) = \{G_2 e^{-(q^2 R_{g2}^2)/3} + B_2 e^{-(q^2 R_{g1}^2)/3} (q_2^*)^{-d_{f2}}\} + \{G_1 e^{-(q^2 R_{g1}^2)/3} + B_1 (q_1^*)^{-1}\} \tag{6}$$

where $q_i^* = [q/\{\mathrm{erf}(qkR_{gi}/\sqrt{6})\}^3]$ and $k \approx 1.06$. The terms in the first bracket with subscript "2" represent the good solvent scaling regime with mass-fractal dimension $d_{f2} \approx 5/3$ and the second bracket with subscript "1" represent the rodlike persistence scaling regime. In each set of brackets, the first term gives the Guinier exponential decay and the second term yields the structurally limited power law. The SANS data, as shown in Figure 2, contains four distinguishable features, each providing two values associated with the q and $I(q)$ positions of these features. At lowest q we observe the plateau $I(q)$ value, G_2, and R_{g2} for the coil. In the scaling regime, the slope and prefactor for the power-law decay are observed. Near the persistence length, a transition in slope is seen with corresponding $I(q)$ and q values. At high q a power-law decay of -1 with a power-law prefactor is observed. These eight observable features are modeled with a six-parameter

Table 1. Characterization of Long-Chain Branching in Dow HDB Samples

sample	LCB/10^3C ^{13}C NMR[a]	M_n (g/mol)[a]	PDI (M_w/M_n)[a]	β	n_{br}	$n_{br,p}$	ϕ_{br}	z_{br} (g/mol)
HDB-1	0.026	39 300	1.98	0.073	0.080 ± 0.004	0.047 ± 0.005	0.10 ± 0.02	$12\,700 \pm 1500$
HDB-2	0.037	41 500	1.93	0.110	0.115 ± 0.005	0.053 ± 0.005	0.14 ± 0.02	$17\,400 \pm 1600$
HDB-3	0.042	41 200	1.99	0.124	0.144 ± 0.007	0.065 ± 0.005	0.17 ± 0.02	$16\,500 \pm 1600$
HDB-4	0.080	39 200	2.14	0.224	0.262 ± 0.007	0.090 ± 0.008	0.28 ± 0.03	$18\,600 \pm 1700$

[a] Reference 22.

function where the variables that are floated while executing the unified fit are C_p, d_f, R_{g2}, B_2, d_{min}, and B_1. All the parameters used in the unified function have been described in detail previously.[3,19]

For a long-chain branched polymer, as shown Figure 1a, branch sites occur along the minimum path through the structure. The average minimum path is composed of segments between branch points or chain ends having an average number of Kuhn steps, $(p/n_{s,p})$, where $n_{s,p}$ is the average number of segments per minimum path. The end-to-end distance of the minimum path, r, in units of number of Kuhn steps can then be given by

$$r = n_{s,p}\left(\frac{p}{n_{s,p}}\right)^{3/5} \tag{7}$$

For a branched polymer chain, r can also be described in terms of p (Figure 1a) as

$$r = p^{1/d_{min}} \tag{8}$$

Equating eqs 7 and 8, we obtain the following relationship:

$$n_{s,p} = \left[p^{(1/d_{min})-(3/5)}\right]^{5/2} \tag{9}$$

The number of branch sites per minimum path is then given by

$$n_{br,p} = n_{s,p} - 1 \tag{10}$$

The average number of Kuhn steps in a segment, $n_{k,s}$, can be described by

$$n_{k,s} = \frac{p}{n_{br,p}+1} = \frac{z}{2n_{br}+1} \tag{11}$$

where n_{br} is the number of branch sites per chain, $n_{br,p}+1$ is the number of segments in the minimum path, and $2n_{br}+1$ is the total number of segments in the polymer.

From eq 3, we can rewrite eq 11 as

$$n_{br} = \frac{z^{[(5/2d_f)-(3/2c)]+[1-(1/c)]}-1}{2} \tag{12}$$

This quantity is equivalent to the average number of branches per chain, β, obtained from NMR.[4,14,22]

The mole fraction branch content, ϕ_{br}, combined with n_{br} can be used to estimate a new quantity, the weight-average branch length (z_{br}), from the following relationship

$$z_{br} = \frac{z\phi_{br}M_{Kuhn}}{n_{br}} \tag{13}$$

where M_{Kuhn} is the mass of one Kuhn step as determined from the Kuhn length, $l_k = 2l_p$, of a polyethylene sample,[3] which is $l_k \times 13.4$ g/(mol Å). The quantity n_{br} obtained from this analysis is compared with β obtained from NMR.[22]

Table 2. Size and Dimensions of Dow HDB Samples Measured from SANS

sample	R_g (Å)	d_f	c	l_p (Å)
HDB-1	95 ± 6	1.70 ± 0.02	1.03 ± 0.01	6.5 ± 0.5
HDB-2	103 ± 8	1.71 ± 0.02	1.04 ± 0.02	6.7 ± 0.4
HDB-3	104 ± 8	1.73 ± 0.02	1.05 ± 0.02	6.6 ± 0.5
HDB-4	79 ± 4	1.78 ± 0.04	1.08 ± 0.03	6.9 ± 0.5

Materials and Methods

We used metallocene-catalyzed model branched polyethylene chains with low degrees of structural branching and narrow molecular weight distributions (Table 1). These samples have been extensively studied and characterized in the literature.[12,13,22] SANS was performed on dilute solutions of these model polyethylenes in deuterated *p*-xylene, which is a good solvent for polyethylene at 125 °C. Deuterated *p*-xylene was purchased from Sigma-Aldrich. The samples were equilibrated at 125 °C for 3 h prior to the measurements to ensure complete dissolution of the solute. 1 wt % solutions were used, well below the overlap concentration as described by Murase et al.[23] as verified by superposition of concentration normalized data from 0.25, 0.5, and 1 wt % for the same polymer solution. SANS experiments were carried out at the Intense Pulsed Neutron Source (IPNS), Argonne National Laboratory, Argonne, and NG-7 SANS[24] at National Institute of Standards and Technology (NIST) Center for Neutron Research (NCNR), Gaithersburg. Standard data correction procedures for transmission and incoherent scattering along with secondary standards were used to obtain $I(q)$ vs q in absolute units.[25] Experimental runs took approximately 4 h per sample at IPNS and 2 h at NIST.

Results and Discussion

Corrected SANS data are plotted in a log−log plot of $I(q)$ vs q, as shown in Figure 2. The data are fit to the unified function (eq 6)[3,17−19] followed by the application of the scaling model.[4] The dotted curve in Figure 2 represents the Guinier exponential decay at low q. The dashed curve in Figure 2 represents the unified fit at the persistence substructural level. As long as reasonable starting values are chosen, for each sample analysis, the unified fit was robust with rapid convergence to the same values. Reasonable starting values can be determined by visually inspecting the four main features of the scattering curve, described above. Table 1 lists the sample names, NMR branch content in terms of number of long-chain branches per 1000 carbon atoms,[22] LCB/10^3C, number-average molecular weight[22] M_n, polydispersity index (M_w/M_n),[22] PDI, and average number of branch sites per chain, β, from NMR.[22] The NMR branch content, in terms of number of long-chain branches per 1000 carbon atoms, is converted to average number of branch sites per chain, β, using the relationship[22]

$$\beta = \frac{(\text{no. of LCB}/1000)_{NMR}M_n}{14000} \tag{14}$$

where M_n is the number-average molecular weight of the polyethylene and 14 000 g/mol refers to the molar mass of 1000 backbone carbons. Table 1 further lists the quantities calculated from SANS including number of branch sites per chain from eqs

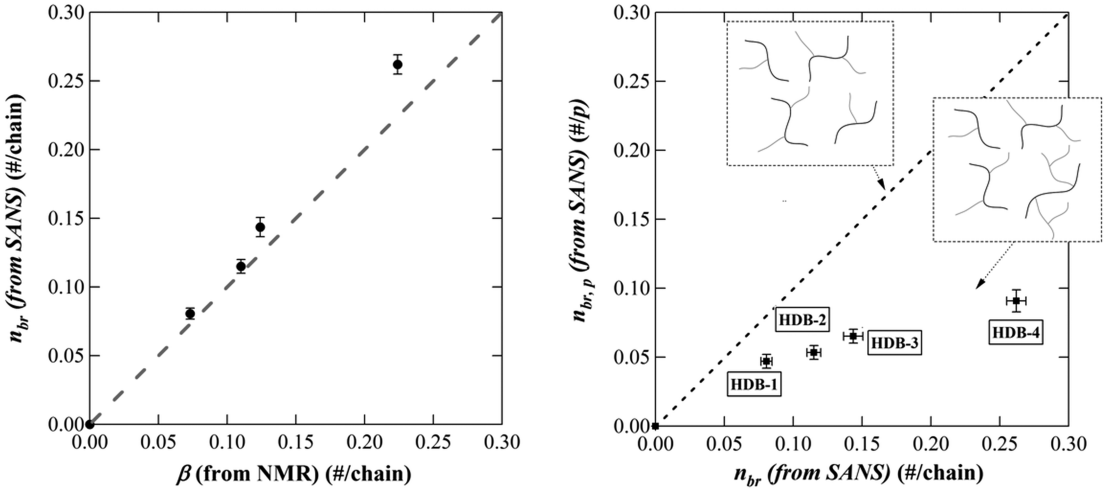

Figure 3. (a, left) Plot of number of branch sites per chain, n_{br}, calculated from eq 12 against average number of branches per chain, β, from NMR.[22] The dashed line represents $n_{br} = \beta$. (b, right) Plot of number of branch sites per minimum path, $n_{br,p}$, calculated from eq 10 against n_{br} calculated from eq 12. The dotted line represents $n_{br} = n_{br,p}$.

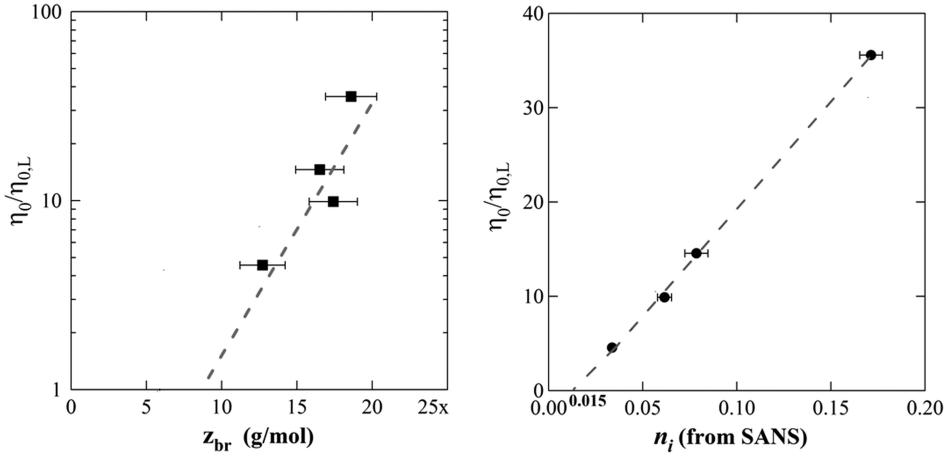

Figure 4. (a, left) Log−linear plot of zero shear rate viscosity enhancement for linear polyethylene of the same M_w[22] against the average length of a branch, z_{br} (from SANS), for the HDB samples. The extrapolation of z_{br} data intercepts the z_{br} axis at 9000 g/mol. (b, right) Linear plot of zero shear rate viscosity enhancement for linear polyethylene of same M_w[22] against number of inner segments per chain, n_i, for the HDB samples. The error in n_i for HDB-1 is smaller than the point size.

9−12, n_{br}, number of branch sites per minimum path from eqs 9 and 10, $n_{br,p}$, mole fraction branches from eq 4, ϕ_{br}, and average branch length from eq 13, z_{br}. Table 2 lists the average radius of gyration of the coil (R_g), mass-fractal dimension, d_f, connectivity dimension, c, and persistence length,[3] l_p, measured from SANS. Errors reported were propagated from the counting error in the raw data.

Figure 3a plots n_{br} calculated from eq 12 against β from ref 22 with good agreement, although the value of n_{br} is slightly higher than β. Figure 3b plots $n_{br,p}$ calculated from eq 10 against n_{br} from eq 12. While n_{br} measures every branch point in a polymer chain, $n_{br,p}$ reflects the number of branch points in the minimum path. For a comb or 3-arm star structure (top inset, Figure 3b), with no branch-on-branch structure, it is expected that $n_{br,p} = n_{br}$. For a more complex structure displaying branch-on-branch topology, $n_{br,p} < n_{br}$. Although we observe a monotonic relationship in the plot, $n_{br,p}$ is lower than n_{br} for the HDB samples. This implies the presence of branch-on-branch architecture in these samples. The plot of $n_{br,p}$ vs n_{br} in Figure 3b shows a stronger deviation at higher branch content. The $n_{br,p}$ value plateaus at about 0.1 while n_{br} increases to almost 0.3. The plateau in $n_{br,p}$ indicates that the minimum path branch content reaches a constant value while additional branches are added through branch-on-branch structures. The system consists of a few hyperbranched chains in a majority of linear chains at high branch content rather than a uniform distribution of branching because n_{br} is less than 1 and due to the noted difference between $n_{br,p}$ and n_{br}.

As mentioned earlier, the average branch length, z_{br}, can have a significant impact on understanding the rheological behavior of long-chain branched polymers. Figure 4a shows a log−linear plot of the zero shear rate viscosity enhancement, $\eta_0/\eta_{0,L}$, as reported by Costeux et al.,[22] versus the average branch length, z_{br}. An exponential increase in the viscosity enhancement with increasing branch length is observed.

The extrapolation of the fit of the data in Figure 4a intercepts the z_{br} axis around 9000 g/mol. This implies that the viscosity enhancement effect due to long-chain branching starts to occur, when the weight-average branch length becomes 9000 g/mol. For model samples with monodisperse branches,[26] it has been previously reported that significant rheological affects are only observed for branches 2.4 times the entanglement molecular weight, M_e, of 1250 g/mol.[13] Since z_{br} is a weight-average branch length, the ratio of z_{br} to the literature value[26] suggests that the higher value in the current analysis can be attributed to the polydispersity in the branch lengths of the HDB samples. This implies a polydispersity index of $M_w/M_n \approx 9000/3000 = 3$ for the branches.

On the basis of previous studies,[22,27] the viscosity enhancement can also be attributed to the number of inner segments per chain, n_i, as described in ref 22, in branch-on-branch polymer chains. n_i can be approximated by

$$n_i = n_{br} - n_{br,p} \quad (15)$$

Figure 4b shows a plot of viscosity enhancement, $\eta_0/\eta_{0,L}$, vs n_i calculated in this way. The plot displays a linear increase in viscosity enhancement with increasing number of inner segments for the samples studied. If the inner segments are considered not to contribute to the viscous response of the melt and since the mole fraction of inner segments in the melt is proportional to n_i, we can consider the polyethylene melt as a dilute solution of n_i inner segments per chain in a melt of mostly linear polyethylene. The linear functionality of $\eta_0/\eta_{0,L}$ in n_i is then analogous to a dilute suspension of particulates. We can use the Einstein approximation[28] for a dilute particulate suspension, $\eta_0 = \eta_{0,L}(1 + n_i[\eta_0])$ as an approximation, except that there is a shift of about 0.015 on the n_i axis. Einstein behavior indicates that inner segments do not contribute to flow, acting as particulate inclusions, and show a simple volumetric exclusion from the remaining viscous material composed of linear chains and non-hyperbranched chains. In the Einstein linear equation the slope, 278 chains/inner segment, corresponds to a type of intrinsic viscosity for hyperbranched structures in a suspension of linear chains. The shift factor of 0.015 inner segments/chain may arise due to the presence of a small population of branched segments that are not long enough to significantly affect viscosity. These are reflected in Figure 4a by the nonzero intercept on the z_{br} axis.

Conclusion

A novel scaling approach to characterize long-chain branch content in polyethylene has been presented. Through this approach, the new quantities mole fraction branch content, ϕ_{br}, number of branch sites per chain, n_{br}, number of branch sites per minimum path, $n_{br,p}$, number of inner segments per chain, n_i, and average branch length, z_{br}, are reported. While ϕ_{br} quantifies the mole fraction long-chain branch content z_{br} can provide additional information about the architectural makeup of a polymer, resulting in improved understanding of its rheological properties. $n_{br,p}$ when combined with n_{br} gives further details about the chain architecture. This information will give polymer and catalyst chemists enhanced information to understand polymer architectures with desirable rheological properties. The approach encompasses both qualitative and quantitative analysis of long-chain branching in polyethylene. The scaling model has been successfully employed previously to determine branching in ceramic aggregates[4] and to quantify the degree of folding in proteins and RNA.[5]

The procedure described in this paper does have certain limitations. First, the system being studied would need to show mass-fractal scaling so it may not be applicable to some densely branched dendritic macromolecules for example. The method is also not able to give a firm value for the length at which a branch becomes a long-chain branch since there may be an overlap regime where both persistence effects associated with SCB (as discussed in ref 3) and scaling effects associated with LCB are observed. The effect of polydispersity in polymers and blending of different systems can be accommodated in this approach and will be discussed in forthcoming papers. The new scaling approach discussed here will be further tested with model star and comb polyethylene samples.

Acknowledgment. We thank L. J. Effler and A. W. deGroot of The Dow Chemical Company for providing the polyethylene samples. This work utilized facilities supported in part by the National Science Foundation under Agreement DMR-0454672. We acknowledge the support of the National Institute of Standards and Technology (NIST), U.S. Department of Commerce, for providing the neutron research facilities used in this work. We are grateful to B. Hammouda, S. Kline, and M. Laver at NIST for their valuable support and guidance during beam time at NIST. We also acknowledge the support of Intense Pulsed Neutron Source (IPNS) and thank P. Thiyagarajan for valuable support during preliminary work. We acknowledge the support of Equistar Chemicals, LP, for funding of this work.

References and Notes

(1) Desimone, J. M. *Science* **1995**, *269* (5227), 1060–1061.
(2) Arneodo, A.; Argoul, F.; Bacry, E.; Muzy, J. F.; Tabard, M. *Phys. Rev. Lett.* **1992**, *68* (23), 3456–3459.
(3) Ramachandran, R.; Beaucage, G.; Kulkarni, A. S.; McFaddin, D.; Merrick-Mack, J.; Galiatsatos, V. *Macromolecules* **2008**, *41* (24), 9802–9806.
(4) Beaucage, G. *Phys. Rev. E* **2004**, *70* (3), 10.
(5) Beaucage, G. *Biophys. J.* **2008**, *95* (2), 503–509.
(6) Bick, D. K.; McLeish, T. C. B. *Phys. Rev. Lett.* **1996**, *76* (14), 2587.
(7) Lohse, D. J.; Milner, S. T.; Fetters, L. J.; Xenidou, M.; Hadjichristidis, N.; Mendelson, R. A.; Garcia-Franco, C. A.; Lyon, M. K. *Macromolecules* **2002**, *35* (8), 3066–3075.
(8) Guan, Z. B.; Cotts, P. M.; McCord, E. F.; McLain, S. J. *Science* **1999**, *283* (5410), 2059–2062.
(9) Everaers, R.; Sukumaran, S. K.; Grest, G. S.; Svaneborg, C.; Sivasubramanian, A.; Kremer, K. *Science* **2004**, *303* (5659), 823–826.
(10) Zimm, B. H.; Stockmayer, W. H. *J. Chem. Phys.* **1949**, *17* (12), 1301–1314.
(11) Yan, D.; Wang, W. J.; Zhu, S. *Polymer* **1999**, *40* (7), 1737–1744.
(12) Wood-Adams, P. M.; Dealy, J. M. *Macromolecules* **2000**, *33* (20), 7481–7488.
(13) Wood-Adams, P. M.; Dealy, J. M.; deGroot, A. W.; Redwine, O. D. *Macromolecules* **2000**, *33* (20), 7489–7499.
(14) Kulkarni, A. S.; Beaucage, G. *J. Polym. Sci., Part B: Polym. Phys.* **2006**, *44* (10), 1395–1405.
(15) Kuhn, W. *Kolloid-Z.* **1934**, *68* (1), 2–15.
(16) Guinier, A.; Fournet, G. *Small Angle Scattering of X-Rays*; Wiley: New York, 1955.
(17) Beaucage, G. *J. Appl. Crystallogr.* **1995**, *28*, 717–728.
(18) Beaucage, G. *J. Appl. Crystallogr.* **1996**, *29*, 134–146.
(19) Beaucage, G.; Rane, S.; Sukumaran, S.; Satkowski, M. M.; Schechtman, L. A.; Doi, Y. *Macromolecules* **1997**, *30* (14), 4158–4162.
(20) Chatterjee, T.; Jackson, A.; Krishnamoorti, R. *J. Am. Chem. Soc.* **2008**, *130* (22), 6934-+.
(21) Sorensen, C. M.; Wang, G. M. *Phys. Rev. E* **1999**, *60* (6), 7143–7148.
(22) Costeux, S.; Wood-Adams, P.; Beigzadeh, D. *Macromolecules* **2002**, *35* (7), 2514–2528.
(23) Murase, H.; Kume, T.; Hashimoto, T.; Ohta, Y.; Mizukami, T. *Macromolecules* **1995**, *28* (23), 7724–7729.
(24) Glinka, C. J.; Barker, J. G.; Hammouda, B.; Krueger, S.; Moyer, J. J.; Orts, W. J. *J. Appl. Crystallogr.* **1998**, *31*, 430–445.
(25) Kline, S. R. *J. Appl. Crystallogr.* **2006**, *39*, 895–900.
(26) Gell, C. B.; Graessley, W. W.; Efstratiadis, V.; Pitsikalis, M.; Hadjichristidis, N. *J. Polym. Sci., Part B: Polym. Phys.* **1997**, *35* (12), 1943–1954.
(27) Read, D. J.; McLeish, T. C. B. *Macromolecules* **2001**, *34* (6), 1928–1945.
(28) Einstein, A. *Ann. Phys.* **1906**, *19*, 289–306.